



Cite this: *RSC Adv.*, 2023, 13, 8944

# Efficient removal of norfloxacin from water using batch airlift-electrocoagulation reactor: optimization and mechanisms analysis†

Xuege Gu, Junfeng Li, \* Xueting Feng, Wenying Qu, Wenhui Wang and Jiankang Wang

In this study, we developed an airlift-electrocoagulation (AL-EC) reactor to remove norfloxacin (NOR) from water. Six parameters influencing NOR removal were investigated, and the possible removal mechanism was proposed based on flocs characterization and intermediates analysis. The performances for treating different antibiotics and removing NOR from 3 types of water were also evaluated. The best NOR removal efficiency was obtained with the iron anode and aluminum cathode combination, a current density of  $2 \text{ mA cm}^{-2}$ , an initial pH of 7, a treatment time of 32 minutes and an air flow rate of  $200 \text{ mL min}^{-1}$ , the supporting electrolyte type was NaCl, and the initial NOR concentration was  $10 \text{ mg L}^{-1}$ . Flocs adsorption and electrochemical oxidation were the main ways to remove NOR from water. The average removal efficiency of the AL-EC reactor exceeded 60% of the different antibiotic concentrations in artificial and real water. The highest NOR removal rate reached 93.48% with an operating cost of  $0.153 \text{ USD m}^{-3}$ . The present work offers a strategy for NOR removal from water with high efficiency and low cost, showing a huge potential for the application of the AL-EC in antibiotic contaminated water treatment.

Received 22nd January 2023

Accepted 13th March 2023

DOI: 10.1039/d3ra00471f

rsc.li/rsc-advances

## 1 Introduction

Over the past few decades, antibiotics have been widely used for treating bacterial infections in humans and animals due to their convenient use and remarkable curative effect. However, only approximately 30% of antibiotics were exhausted by humans and animals, and approximately 70% of them were discharged into the environment in the form of metabolites with unchanged structure. Antibiotics also pollute the water environment through the discharge of wastewater in hospitals and pharmaceutical factories effluents, and their concentrations can reach the  $\mu\text{g L}^{-1}$ , even  $\text{mg L}^{-1}$  level.<sup>1,2</sup> As one of the most consumed antibiotics in the world, norfloxacin (NOR) in aquatic ecosystems poses a huge environmental risk, including the inhibition of animal and plant growth<sup>3</sup> and the increase of resistant bacteria and resistance genes.<sup>4</sup> Therefore, finding an effective technique to remove NOR from wastewater is necessary. Previous studies have developed some techniques to remove antibiotics from wastewater, including adsorption,<sup>5</sup> coagulation,<sup>6</sup> electrochemical oxidation,<sup>7,8</sup> UV irradiation<sup>9</sup> and ultrasonic radiation.<sup>10</sup> Although some of those techniques are effective, some disadvantages limit their large-scale application

in practice, such as relatively higher operating costs, extra chemicals addition, and complex treatment conditions.

Generally, electrocoagulation (EC) technique uses metals (iron or aluminum) as the sacrificial anode, metal ions are released when applying current between anodes and cathodes. These ions were hydrolyzed to form metal hydroxide and complexes, and pollutants in the solution were removed by adsorption, neutralization and co-precipitation.<sup>11</sup> Therefore, the simple, efficient, low-cost EC method is ideal for treating antibiotic-containing wastewater.

Most EC reactors used in laboratory and industrial scales were tanks with electrodes inserted, lacking contact with coagulants and pollutant particles. Thus, the mechanical mixer is used to increase the mixing efficiency. However, the excessive shear force caused by mechanical stirring would lead to the irreversible break up of flocs<sup>12</sup> and consume extra energy. At the same time, a type of reactor called airlift reactor has also attracted people's attention. It can be seen as a modified bubble column reactor by inserting cylindrical or rectangular plates inside the column to separate the fluid into two zones, riser and downcomer.<sup>13</sup> Bubbles floated in the riser section, which led to a pressure difference between the riser and downcomer sections, forming liquid circulation.<sup>14</sup> This kind of circulation presented lower and more homogeneous shear stress, which is suitable for fragile flocs. Moreover, the airlift reactor is not involved with moving parts, making it simple to construct and operate with low power consumption. Therefore, some researchers began to combine EC with airlift reactors as airlift-

College of Water Conservancy and Architectural Engineering, Shihezi University, Shihezi, 832000, PR China. E-mail: lijfshz@126.com

† Electronic supplementary information (ESI) available. See DOI: <https://doi.org/10.1039/d3ra00471f>



electrocoagulation (AL-EC) reactors and obtained good efficiency in treating dye,<sup>15</sup> oil,<sup>16</sup> fluorine,<sup>17</sup> arsenic<sup>18</sup> and chemical oxygen demand (COD)<sup>19</sup> from wastewater. Another reason for the good performance of AL-EC was the addition of air. Aeration offered some advantages, such as reduced passivation of electrodes and enhanced oxidation process. It has been reported that aeration in the EC process can increase decolourization and COD removal efficiency of dye wastewater<sup>20</sup> and arsenic removal efficiency of polluted groundwater.<sup>21</sup>

To date, very few researches reported the treatment of NOR by EC,<sup>22</sup> and the mechanism for the removal of NOR by AL-EC is not clear yet, and further research is needed.

Therefore, this study developed an AL-EC reactor to remove NOR from water and aims to: (1) evaluate the effect of different operating parameters (current density, solution pH, air flow rate, electrode combination, supporting electrolyte types, and initial NOR concentration) on the NOR removal process; (2) character and analyse the flocs and solutions, elucidate the NOR removal mechanism; (3) remove NOR from real water and treat different types of antibiotics, evaluate the treatment costs.

## 2 Materials and methods

### 2.1 Chemicals and materials

Norfloracin ( $C_{16}H_{18}FN_3O_3$ , 99%), hydrochloric acid (HCl, 36%), sodium hydroxide (NaOH, 99%), sodium chloride (NaCl, 99%), potassium chloride (KCl, 99%), sodium sulphate ( $Na_2SO_4$ , 99%), Tetracycline ( $C_{22}H_{24}N_2O_8$ , 99%), Metronidazole ( $C_6H_9N_3O$ , 99%) were purchased from Beijing Chemical Reagent Factory China (Beijing, China). All chemicals used were analytical grade. The electrodes were the A3 iron plates and 6061 aluminum plates with over 99% iron or aluminum contents.

### 2.2 Airlift-electrocoagulation reactor and procedure

The schematic diagram of the AL-EC reactor used for this study is shown in Fig. 1. The device was constructed by the acrylic board with a size of  $16 \times 6 \times 16.5$  cm and a working volume of 1000 mL. It also included air pump, gas flowmeter, and bubble diffuser. Three pieces of metal plate electrodes (iron or aluminum) were vertically arranged in the cell. One anode was placed between the two cathodes to ensure that the current and

potential on the anode distributes uniformly. The electrode size was  $8 \times 10.5 \times 0.3$  cm, the distance between the electrodes was set to 1 cm, and the effective electrodes area was about  $150 \text{ cm}^2$ . The electrodes were connected in monopolar parallel mode with a DC power supply unit (MS-155D). The electrodes were polished with sandpaper and rinsed with 1% HCl solution and distilled water for removing oxides film before every run.

The pH of synthetic solutions were measured by pH meter (Sanxin WS100) and adjusted to set values by  $0.1 \text{ mol L}^{-1}$  HCl or NaOH diluted solution. The valve of the air flow meter was set to the desired flow rate (when the air flow rate is set to  $0 \text{ mL min}^{-1}$ , it is not aerated). When the steady state attained after few minutes, the power supply was turned on at the required settings of voltage/current. Samples were taken regularly (every 4 minutes) from the reactor and filtered through  $0.45 \mu\text{m}$  micron filters before analysis. Dissolved oxygen concentrations were measured by multi-parameter water quality analyzer (HQ30d, HACH) with dissolved oxygen electrode (LDO10101, HACH). Electrodes were weighted before and after the treatment process. Sludge was dried at in a vacuum drying oven (YLD-2000) until constant weight and collected for further analysis.

### 2.3 Analysis

NOR concentration was determined at wavelength of 277 nm with ultraviolet and visible spectrophotometer (DR6000, HACH).

The removal efficiency of NOR was calculated by the following eqn (1):

$$\text{Removal efficiency(\%)} = \frac{C_0 - C_t}{C_0} \times 100 \quad (1)$$

where,  $C_0$  is the initial and  $C_t$  is the final NOR concentration ( $\text{mg L}^{-1}$ ) in solution.

The current density  $j$  ( $\text{mA cm}^{-2}$ ) was calculated according to the following eqn (2):

$$j = \frac{I}{S} \quad (2)$$

where  $I$  is the applied current (mA) and  $S$  is the effective surface area of the anode ( $\text{cm}^2$ ).

During the electrocoagulation process, the amount of dissolved electrode (anode) can be described by Faraday's Law of Electrolysis:

$$W = \frac{I \times t \times M}{Z \times F} \quad (3)$$

where  $W$  is the experimentally observed mass (g),  $I$  is the current intensity (A),  $t$  is the electrolysis time (s), and  $M$  is the molar mass of the metal ( $\text{g mol}^{-1}$ ),  $Z$  is the number of electrons involved in the redox reaction ( $Z = 2$  for iron),  $F$  is Faraday's constant ( $96485 \text{ C mol}^{-1}$ ).

The energy consumption of electrodes during the EC process was calculated using the following eqn (4):

$$E_c = \frac{T \times i \times U}{V_1 \times (C_0 - C_1)} \quad (4)$$

where  $T$  is the electrolysis time (h),  $i$  is the applied current (mA) and  $U$  is applied voltage (V),  $V_1$  is the treated solution volume

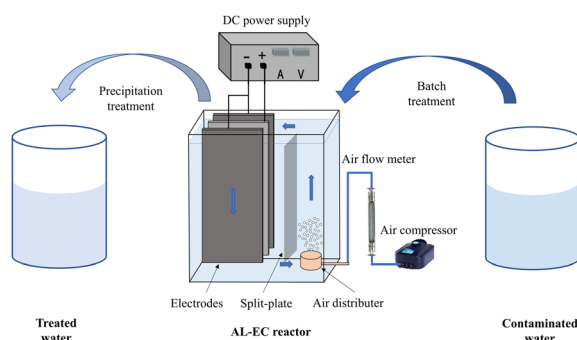


Fig. 1 Schematic diagram of the airlift electrocoagulation reactor.



( $\text{m}^3$ ),  $C_0$  is the initial and  $C_t$  is the final NOR concentration ( $\text{mg L}^{-1}$ ) in solution.

The amount of sludge generated during the EC process was evaluated by sludge produced per NOR removed as  $\text{g mg}^{-1}$ , calculated using the following eqn (5):

$$S_v = \frac{m}{V_2 \times (C_0 - C_t)} \quad (5)$$

where  $m$  is the weight of dry sludge (g),  $V_2$  is the treated solution volume (L),  $C_0$  is the initial and  $C_t$  is the final NOR concentration ( $\text{mg L}^{-1}$ ) in solution.

A scanning electron micrograph-energy dispersive spectrometry (SEM) and X-ray fluorescence (XRF) (FEI Quanta 650, Thermo Fisher, U.S.A.) was used to characterize the morphology and mineralogical composition of flocs before and after aeration. The surface chemical functional groups of the flocs were performed using Fourier transform infrared spectroscopy (FT-IR) (Thermo Scientific Nicolet Summit, USA). X-ray diffraction (XRD) (D8 Advance, Bruker, Germany) was used to analyse the flocs' crystal structure. High-performance liquid chromatography-mass spectrometry (LC-MS) (Shimadzu, LCMS-9030, Japan) was used to identify the degradation intermediates of NOR.

### 3 Effect of operating parameters

#### 3.1 Effect of electrode combinations

Fig. 2(a) shows the NOR removal performance of different electrode combinations at the same current densities (2 mA

$\text{cm}^{-2}$ ) at initial pH 7. It can be seen that the Fe anode and Al cathode combination had the highest NOR removal efficiency, reaching 93.48% after 32 minutes of treatment, while the Al anode and Fe cathode, Al anode and Al cathode, and Fe anode and Fe cathode combination were 82.84%, 80.31%, 70.13%, respectively.

The specific energy consumption and sludge amount of different electrode combinations were shown in the Fig. 2(b). Maximum specific energy consumption was observed to be  $64.65 \text{ kW h kg}^{-1}$  with Fe anode and Fe cathode combination after 40 minutes of treatment. It also formed the most sludge, up to  $0.42 \text{ g mg}^{-1}$ . Fig. 2(b) also shows that all Fe anode combinations produced more sludge than aluminium anodes. Iron is less conductive than aluminium, so it requires a higher voltage at the same current density,<sup>23</sup> led to Fe electrode combinations consumed more energy than Al electrode.

According to Faraday's law, the amount of coagulant metal dissolved is inversely proportional to the number of electrons lost and directly proportional to the molar mass of the metal. Fe loses fewer electrons in the reaction, and its molar mass is twice that of aluminium. Thus, Fe electrodes formed more coagulant to absorb pollutants and also produced more sludge. The formation of a tight layer of  $\text{Al}_2\text{O}_3$  during the process limited the dissolution of the Al anode combinations,<sup>24</sup> resulting in a low level of removal efficiency and low sludge yield. It also observed that denser bubbles formed on the Al cathode surface through the Fe anode and Al cathode combination. It is reported that

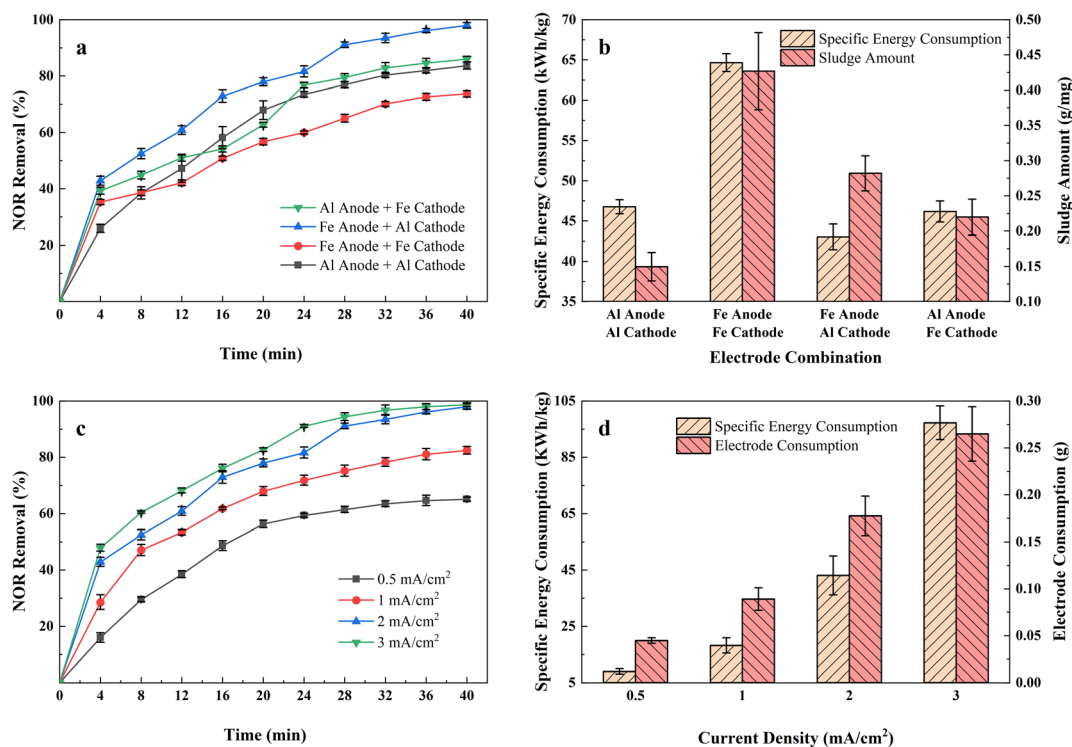


Fig. 2 (a) Influence of different electrode combinations on NOR removal; (b) energy consumption and sludge volume of different electrode combinations; current density =  $2 \text{ mA cm}^{-2}$ , initial pH = 7, flow rate =  $200 \text{ mL min}^{-1}$ , initial NOR concentration =  $10 \text{ mg L}^{-1}$ ; (c) influence of applied current density on NOR removal; (d) energy and electrode consumption of different current density; electrode combination, Fe anode and Al cathode, initial pH = 7, flow rate =  $200 \text{ mL min}^{-1}$ , initial NOR concentration =  $10 \text{ mg L}^{-1}$ .



smaller bubbles can promote the combination of the metal flocs and the pollutants, improving the removal efficiency.<sup>25</sup>

Therefore, considering the balance of power consumption, NOR removal efficiency, and sludge production, Fe anode and Al cathode were considered the best combination for further research.

### 3.2 Effect of current density

Applied current density refers to the ratio of applied current and electrode area. It is one of the most significant parameters affecting the EC process, for it determined the amount of metal dissolved in solutions and hence affected the formation of coagulants. Fig. 2(c) revealed the NOR removal rate in the airlift-electrocoagulation reactor with time at different current densities (in the range of 0.5–3 mA cm<sup>-2</sup>). The results showed that the NOR removal rate increased with the current density when raising current density from 0.5 to 3 mA cm<sup>-2</sup> improved the removal efficiency from 65.08% to 98.68%.

According to Faraday's Law, more metals and hydroxyl will be produced applying a higher current to form coagulants and remove pollutants.<sup>26</sup> It would also generate more H<sub>2</sub> bubbles from the cathode that capture pollutants, improving solution mixing and mass transfer near the electrode.<sup>27</sup> More active species would also generate from the anode that accelerates chemical oxidation reaction, but some researchers noted that would lead to an increase in by-products and higher

environmental risks.<sup>28,29</sup> If the applied current is too high, it may lead to electrode passivation and increased polarization,<sup>30</sup> leading to an increase in power consumption.<sup>31</sup>

Removal rates increased rapidly for the first 20 minutes at all different current densities. However, the continued application of current did not result in a more significant increase in removal efficiency, and additional energy and electrode materials were consumed. Fig. 2(d) displays the calculated quantity of iron electrode consumed (g) and energy consumption for 40 minutes of treatment at different current densities. It demonstrated that specific energy consumption increased vertically from 8.90 to 97.22 kW h kg<sup>-1</sup> when the current density increased from 0.5 to 3 mA cm<sup>-2</sup>, and the dissolved iron electrode consumed from 0.045 to 0.265 g. Considering the balance between removal efficiency, electrode consumption, and energy consumption, a current density of 2 mA cm<sup>-2</sup> was used in subsequent experiments.

### 3.3 Effect of solution pH

The solution pH is considered one of the critical parameters affecting the performance of the EC process, mainly affecting the speciation of coagulating agents and pollutants. The NOR removal rates and the values of pH changes in the solution are shown in Fig. 3. The results showed that the most favorable pH value for NOR removal was between 7 and 8, consistent with

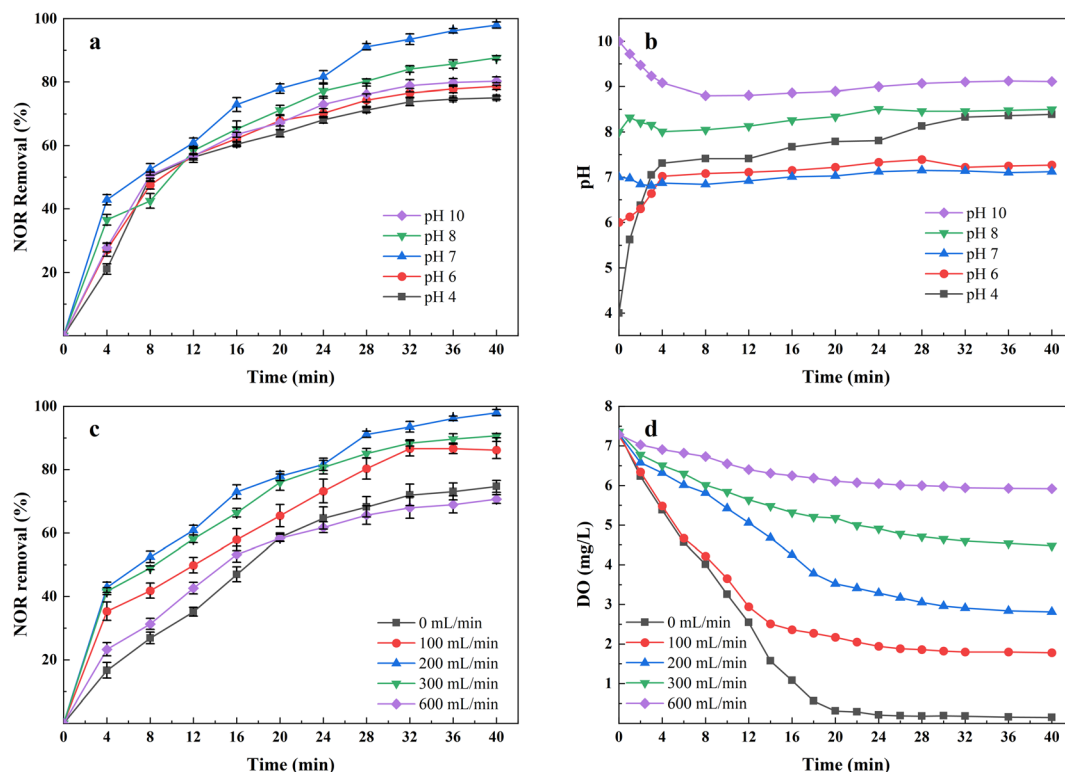


Fig. 3 (a) Influence of difference initial pH on NOR removal; (b) pH values in the process with different initial pH; electrode combination, Fe anode and Al cathode, current density = 2 mA cm<sup>-2</sup>, flow rate = 200 mL min<sup>-1</sup>, initial NOR concentration = 10 mg L<sup>-1</sup>; (c) influence of difference air flow rate on NOR removal; (d) dissolve oxygen concentration in the process with different air flow rate; electrode combination, Fe anode and Al cathode, current density = 2 mA cm<sup>-2</sup>, initial pH = 7, initial NOR concentration = 10 mg L<sup>-1</sup>.



other researches,<sup>32,33</sup> the electrocoagulation using iron anodes performed better in neutral and slightly alkaline conditions.

At a low pH, soluble  $\text{Fe}^{2+}$  and  $\text{Fe}^{3+}$  were dominant in the solution.<sup>34</sup> At the same time, in acid conditions, the rate of  $\text{Fe}^{2+}$  oxidation to  $\text{Fe}^{3+}$  was lower than that in neutral and alkaline conditions,<sup>35</sup> forming less insoluble  $\text{Fe}(\text{OH})_{3(\text{s})}/\text{FeOOH}_{(\text{s})}$  coagulants and therefore, NOR removal decreases. Additionally, At pH above 8, more iron hydroxide complexes like  $\text{Fe}(\text{OH})_4^-$  (ref. 36) and  $\text{Fe}(\text{OH})_6^{3-}$  (ref. 37) formed by continuously consuming  $\text{OH}^-$ , which explained why the solution pH decreased during the initial 5 minutes treatment at pH = 10, in Fig. 3(b). But these ions are useless to the treatment since their poor coagulation performance. Hydroxide ions would be oxidized at the anode and reduced anode dissolution at a high pH range, also decreasing removal efficiency.<sup>38</sup>

Fig. 3(b) also indicates that the solution pH during the electrocoagulation process almost does not change when the initial pH is between 7 and 8. This may be concluded to the produced  $\text{OH}^-$  has completely reacted with the iron and aluminium ions to form various complexes.<sup>39</sup> As shown in Fig. 3(b), the pH of the solution rose rapidly within 5 minutes under acidic conditions, that's because the electrocoagulation reactor was capable of producing enough  $\text{OH}^-$  ions that compensate the acid-buffer and make the solution alkaline.

Therefore, all subsequent tests were conducted under the condition of neutral pH.

### 3.4 Effect of air flow rate

To evaluate the effect of the air flow rate on NOR removal efficiency, the experiments were investigated by varying air flow rate from 0 to 600  $\text{mL min}^{-1}$ , while keeping other operation parameters constant (pH = 7, initial NOR concentration 10  $\text{mg L}^{-1}$ , current density 2  $\text{mA cm}^{-2}$ ). As shown in Fig. 3(c), the highest NOR removal efficiencies were found to be 97.97% with air flow rate of 200  $\text{mL min}^{-1}$ , and then 90.68% with air flow rate of 300  $\text{mL min}^{-1}$ , 86.15% with air flow rate of 100  $\text{mL min}^{-1}$ , 74.67% with air flow rate of 0  $\text{mL min}^{-1}$ . However, the removal efficiency dropped to 70.66% when applying 600  $\text{mL min}^{-1}$  air flow rate. In addition, the colour of solutions changed from deep green to reddish brown when air flow rate changed from 0  $\text{mL min}^{-1}$  to 600  $\text{mL min}^{-1}$ . The dissolved

oxygen concentration with treatment time at each aeration rate was measured and shown in Fig. 3(d).

Properly increased air flow rate can significantly enhance NOR removal efficiency. The air flow raising up, formed turbulence, which improved the mixing condition of the solutions, increased the collision probability between the pollutants and flocs,<sup>40</sup> and made the pollutants captured more effectively. Also, the turbulence reduced the passivation layer on the electrodes, thereby enhancing the transport of ions between the electrodes. Meanwhile, during the EC process, the metal-hydroxide flocs formed at electrode surfaces,<sup>36</sup> and the released gases accumulated at the electrode surface, increased the electrical resistance between the electrodes,<sup>41</sup> leading to bad performance and extra energy consumption. The air flow increased the flow velocity to enhance hydrodynamic scouring,<sup>42</sup> and the effect of air bubbles and deposits was reduced. As shown in Fig. 3(d), different air flow rate affected the dissolved oxygen concentration in solutions, which influenced the redox potential of solutions and, therefore the ratio of  $\text{Fe}^{2+}/\text{Fe}^{3+}$  in the solutions. Higher dissolved oxygen levels helped  $\text{Fe}^{2+}$  oxidize rapidly to  $\text{Fe}^{3+}$ , consistent with the observation of solution colour change. The capacity for forming hydrates is stronger for  $\text{Fe}^{3+}$ , it further reacts with  $\text{OH}^-$  to form  $\text{Fe}(\text{OH})_3$  floc with a large surface area,<sup>20</sup> absorbing more pollutant molecules. At the same time, a higher air flow rate can also promote the production of some reactive oxygen species, accelerate the decomposition of pollutants, and improve efficiency.

The decrease of removal rate in the case of high air flow could be attributed to excessive aeration breaking up the formed flocs,<sup>43</sup> which pollutants absorbed in the EC process were released to solutions. It also led to an increase in suspended solids concentration. In the case of low or no air flow rate, the limited oxidation rate of  $\text{Fe}^{3+}$  ions may result in bad NOR removal efficiency.

### 3.5 Effect of supporting electrolyte types

The addition of supporting electrolyte in the electrocoagulation process to increase the conductivity of the solution to reduce ohmic drop, so as to reduce power consumption and improve efficiency. Therefore,  $\text{Na}_2\text{SO}_4$ ,  $\text{NaCl}$ , and  $\text{KCl}$  were used as supporting electrolytes in the experiments to investigate the

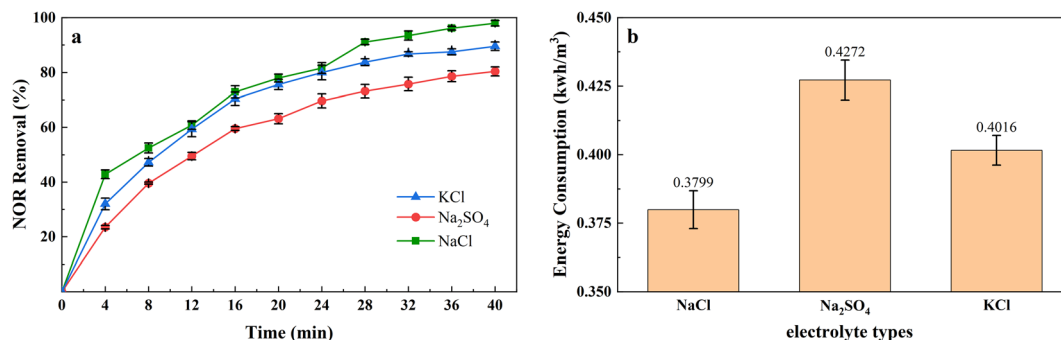


Fig. 4 (a) Influence of different supporting electrolytes on NOR removal; (b) influence of different supporting electrolytes on energy consumption; electrode combination, Fe anode and Al cathode, current density = 2  $\text{mA cm}^{-2}$ , initial pH = 7, air flow rate = 200  $\text{mL min}^{-1}$ , initial NOR = 10  $\text{mg L}^{-1}$ .



effect of supporting electrolyte type on the removal efficiency and energy consumption, and results were shown in Fig. 4(a). The quantity of adding NaCl, Na<sub>2</sub>SO<sub>4</sub>, and KCl was 0.5, 1.215, and 0.6378 g L<sup>-1</sup>, corresponding to 17.11 mM of ions.

It showed the performances of the electrolyte species at 2 mA cm<sup>-2</sup> current density, and it can be seen that the removal rate is higher for NaCl and KCl than that for Na<sub>2</sub>SO<sub>4</sub>, achieved 97.97%, 89.56%, and 80.34%, separately. The better performance for NaCl and KCl was attributed to the Cl<sup>-</sup> formed active chlorine species, they can participate in the oxidation of organic pollutants and ferrous ions.<sup>44</sup> A report showed that a high concentration of Na<sub>2</sub>SO<sub>4</sub> would react with iron hydroxides, decrease the amount of coagulant,<sup>45</sup> and reduced the removal efficiency. In addition, the conductivity of NaCl and KCl was higher than that of Na<sub>2</sub>SO<sub>4</sub> at the same ions intensity, and the required voltage will be much lower,<sup>46</sup> which explained using Na<sub>2</sub>SO<sub>4</sub> as supporting electrolyte consumed more energy in Fig. 4(b).

Although adding the Cl<sup>-</sup> can prompt the oxidation capacity, the degradation by-products could be more toxic than the parent pollutants.<sup>47</sup> Moreover, excessive Cl<sup>-</sup> may accelerate the corrosion pitting rate that leads to overconsumption of Fe<sup>48</sup> and Al<sup>49</sup> electrodes. We need to control the amount of electrolyte added to the solution, which is limited to 0.5 g L<sup>-1</sup> of NaCl in this study.

### 3.6 Effect of initial concentration

Different initial concentrations of NOR from 10 to 100 mg L<sup>-1</sup> were selected for the experiment, and the current density was 2 mA cm<sup>-2</sup>. As shown in Fig. 5, the ratio of sludge produced to NOR removed increased from 0.28 to 0.42 g mg<sup>-1</sup>. Higher initial concentration results in greater NOR removal. However, the residual NOR concentration increased from 0.20 to 2.53 mg L<sup>-1</sup> when NOR concentration was increased from 10 to 100 mg L<sup>-1</sup>. Residual NOR cannot be removed further and remains at a high concentration.

It was due to the same amount of iron hydroxide complexes were generated at the same treatment time and current density,

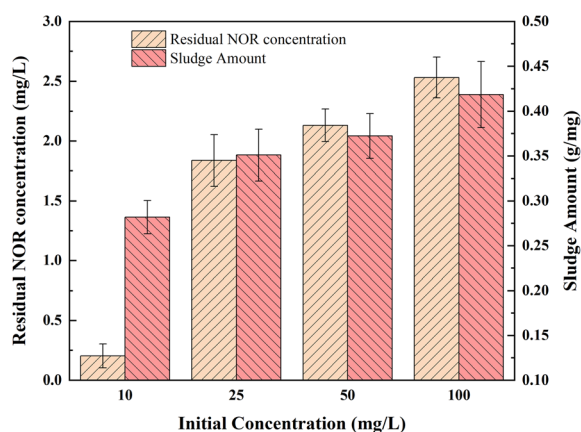


Fig. 5 Influence of different initial concentration on NOR removal; electrode combination, Fe anode and Al cathode, current density = 2 mA cm<sup>-2</sup>, initial pH = 7, air flow rate = 200 mL min<sup>-1</sup>.

the coagulants formed at high NOR concentration were insufficient to adsorb all of the NOR molecules of the solution. Another explanation for removal efficiency decreasing is probably due to the metal hydroxide flocs that trap pollutants molecules lack active sites.<sup>50</sup> For solutions with high initial pollutants concentrations, could achieve better removal efficiencies by diluting solutions.<sup>51</sup>

## 4 Mechanism of NOR removal in AL-EC reactor

### 4.1 Characterization of flocs

Flocs generated from the process under the aeration and non-aeration condition using an AL-EC reactor were characterized by SEM-XRF, FTIR, and XRD.

The morphological characteristics and its elements content are presented in Fig. 6. The morphologies of the flocs under 500 00× and 1 000 00× magnification are shown in Fig. 6(a)–(d) with the consistency of regular particles. As shown in Fig. 6(a) and (b), the flocs formed under aeration conditions had a rough and porous surface, loose structure, and large surface area, which is beneficial to the adsorption of NOR. Under the non-aeration

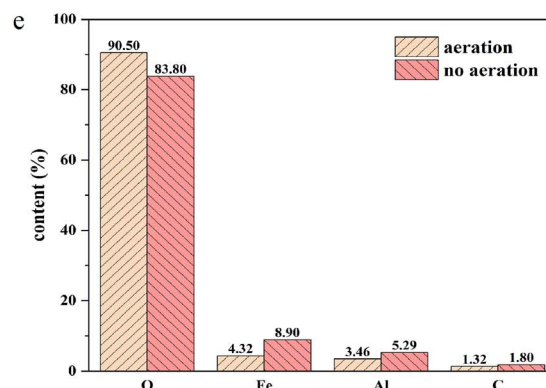
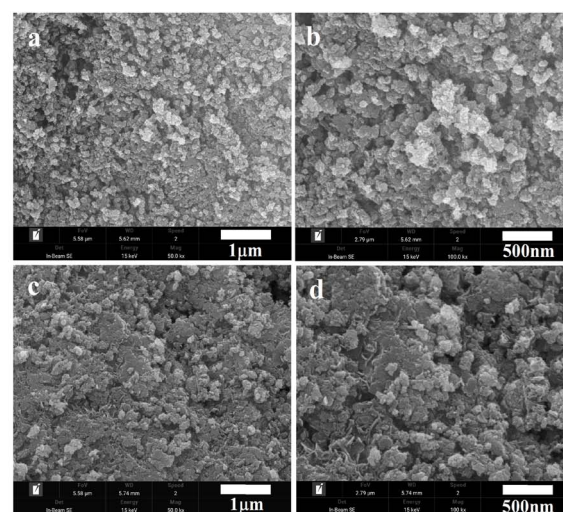


Fig. 6 SEM and XRF analysis of flocs generated from EC treatment by AL-EC reactor in aerated and non-aerated condition for NOR removal.



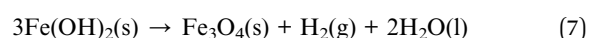
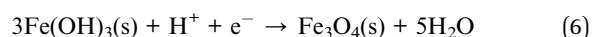
condition, the floc surface was relatively flat and lacked a porous and loose structure (Fig. 6 (c) and (d)).

The XRF (Fig. 6(e)) revealed the component elements and content in the flocs, the main constituent elements were O, Fe, Al, C. The flocs produced under aeration had a higher O content and lower Fe content, with 90.50% and 4.31% compared to 83.80% and 8.90%, it indicated that aeration enhanced the oxidation of flocs and produced more iron oxides. At the same time, the contents of Al in aerated and non-aerated flocs were 3.46% and 5.29%, respectively. This can be explained that the chloride ions added in the solution caused pitting corrosion of the electrode, and part of the Al in the cathode was also dissolved in the solution, according to the previous research results.<sup>52</sup> Iron and aluminium ions formed a series of mono or multi-core metal hydroxyl complexes in the reactor and removed NOR.

As seen in Fig. 7(a), the peak shapes of FTIR for aerated and non-aerated flocs were very similar, with five characteristic peaks. The strong and wide absorption bands near  $3437\text{ cm}^{-1}$  are attributed to the stretching vibration of  $\text{-OH}$  and water molecules,<sup>53</sup> indicating the existence of hydroxide and water molecules in the flocs. The characteristic peak at  $560\text{ cm}^{-1}$  corresponds to  $\text{Fe-O}$  bond,<sup>54</sup> and it can be inferred that both aerated and non-aerated flocs contain iron oxide compounds. From  $1300$  to  $1670\text{ cm}^{-1}$ , both flocs and NOR showed resemble peak shapes, peaks appeared at  $1633$ ,  $1489$ ,  $1382\text{ cm}^{-1}$ , corresponding to the characteristic peaks of  $\text{C=O}$ , aromatic  $\text{C=C}$  bond<sup>55</sup> and  $\text{-COO}^-$  group,<sup>56</sup> respectively. It indicated the formation of interaction between NOR's functional groups and

flocs. From the FTIR results, it can be inferred that during in EC process formed flocs composed of iron hydroxide, and bonded to the NOR's functional groups on the surface. The NOR was mainly removed through complexation and physical adsorption, then precipitated together with flocs.

The crystal structures of the two flocs are shown in Fig. 7(b). Both flocs showed broad peaks but no significant sharp characteristic diffraction peaks, it is indicated that flocs were amorphous structures. The formation of nano-sized metal particles and the high hydration of metal hydroxide floc can explain the poor crystallization.<sup>57</sup> In both aerated and non-aerated conditions, flocs eventually converted into magnetite ( $\text{Fe}_3\text{O}_4$ ), which can be formed by the following reactions (eqn (6) and (7)).<sup>58,59</sup>



Those iron hydroxides with richer hydroxyl function groups and larger specific surface areas formed in the EC process, which achieved the ability to absorb pollutants.

## 4.2 Possible degradation pathways of NOR

Under the condition of aeration and the existence of chlorine electrolyte, active substances such as  $\text{ClO}^\bullet$  and  $^\bullet\text{OH}$  can be produced, which can occur oxidation reactions with NOR and form some intermediates. The degradation intermediates in the treatment process were identified using the LC-MS. As seen in Fig S1,<sup>†</sup> different peaks appeared as the reaction progressed, indicating intermediate formation. Based on the literature review and comparative analysis of mass-charge ratio ( $m/z$ ), eight intermediate products were determined, as shown in Table S1.<sup>†</sup>

In general, NOR could be degraded through the substitution, hydroxylation, decarboxylation, and oxidation of the amino group of the piperazine ring in the following pathways (Fig. 8). Piperazine ring was first oxidized to open the ring,<sup>60</sup> lost the  $\text{-C}_2\text{H}_2\text{-}$  group, and formed the intermittent product M1 ( $m/z = 294$ ). Then in pathway I, it underwent decarboxylation and transformed to M2 ( $m/z = 248$ ), M2 lost ethyl group<sup>61</sup> and further oxidized to M3 ( $m/z = 220$ ). In the Pathway II, M1 can be first converted into M4 ( $m/z = 251$ ) and then further into M5 ( $m/z = 236$ ) by losing amino group.<sup>62</sup> Hydroxyl groups can also

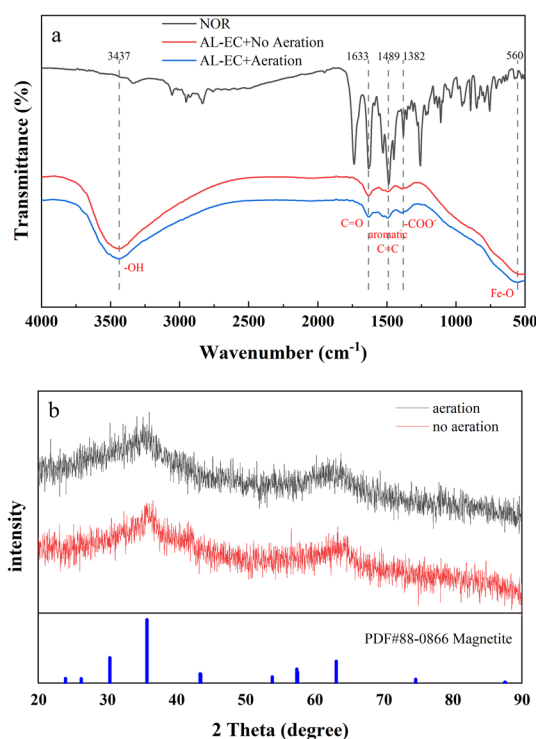


Fig. 7 FTIR and XRD analysis of flocs generated from EC treatment by AL-EC reactor in aerated and non-aerated condition for NOR removal.

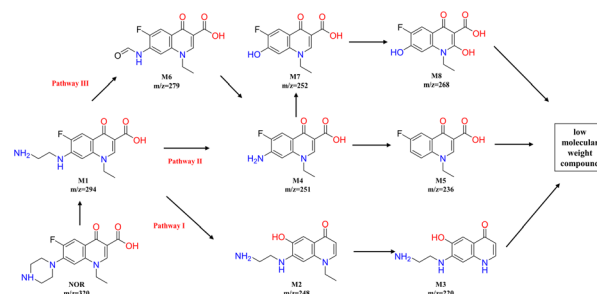


Fig. 8 The possible NOR degradation intermediates and pathway.



substitute the amino groups in the benzene ring of M4 to form M7 ( $m/z = 252$ ), and M7 was further oxidized from M8 ( $m/z = 268$ ). In addition, in pathway III, M4 can also generate from M6 ( $m/z = 236$ ), which was formed by M1 and lost a  $C_2H_5N$  group.<sup>7</sup> As the oxidation process continues, those intermediates can be further degraded to low molecular weight compounds.

### 4.3 Removal mechanism of NOR

Based on the above experiment investigation and analysis, the removal mechanism of NOR by AL-EC with iron and aluminium electrode were proposed and shown in Fig. 9.

**4.3.1 Electrochemical oxidation.** Dissolved oxygen and chlorine-containing electrolyte generated active oxidation species (ROS) with current applied. These active components oxidized NOR and formed smaller molecular weight intermediates. Some of the intermediates can be captured by the flocs.

**4.3.2 Flocs adsorption.** The dissolution of anode metal and the pitting corrosion of cathode metal by chloride ions lead to the release of metal ions into the solution, and formed metal (hydro)oxides flocs with larger surface area. These metal oxides flocs ( $Al(OH)_3$ ,  $Fe(OH)_2$ ,  $Fe(OH)_3$ ,  $Fe_3O_4$ ) can absorb NOR and its' intermediate and then aggregate to form precipitates. Meanwhile, the hydrogen bubbles produced by the cathode and the tiny bubbles of aeration also contribute to removing the precipitates.

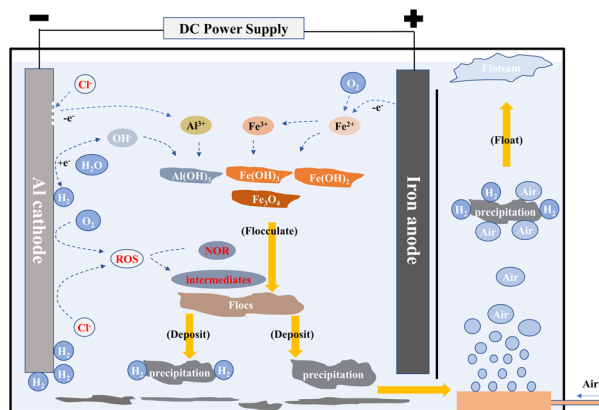


Fig. 9 Mechanism of NOR removal by AL-EC.

## 5 Application and cost evaluation

### 5.1 Efficiency of AL-EC reactor for different antibiotics and removal NOR in different types of water

In order to evaluate the performance of the AL-EC reactor in practical application, the treatment of different kinds of antibiotics and the influence of different water types on NOR removal were studied, as shown in Fig. 10.

Antibiotics such as Tetracycline (TC)<sup>63,64</sup> and Metronidazole (MNZ)<sup>65</sup> were reported can be removed in other electrocoagulation systems by oxidation and adsorption process. Therefore, TC and MNZ were chosen as model pollutants and evaluated their removal efficiency. As shown in Fig. 9(a), all three antibiotics achieved a removal efficiency of over 80%. The highest was NOR, followed by TC and MNZ, which were 85.27% and 82.47%, separately. The above results showed that using the AL-EC reactor to remove varieties of antibiotics from wastewater can exhibit good performance.

These experiments were carried out in synthetic wastewater that dissolved antibiotics in deionized water. Compared to deionized water, groundwater, and river water consists of some extra ions such as chloride and carbonates that may compete with antibiotic molecules in solution, which decreases the removal efficiency. As seen in Fig. 9(b), when the solutions were replaced from deionized water with groundwater and river water, the removal efficiency of NOR dropped from 97.97% to 85.64% and 71.66%. Besides the adsorption competition during the NOR removal process, the lower efficiency may be due to the complexity of river water. But in the EC process, sufficient iron hydroxides were formed to absorb the contaminants and still remained above 70% removal efficiency.

The results above proved the high removal efficiency of the AL-EC reactor for different antibiotics and removal the NOR in different types of water, which means it had universality and adaptability in practical application.

### 5.2 Evaluation of operating cost of AL-EC

The operation cost of the water treatment process is one of the important factors to be considered in practical applications, so it is necessary to evaluate the operating cost.

The operation cost is composed of three parts, the electric energy consumption of aeration and electrocoagulation, the

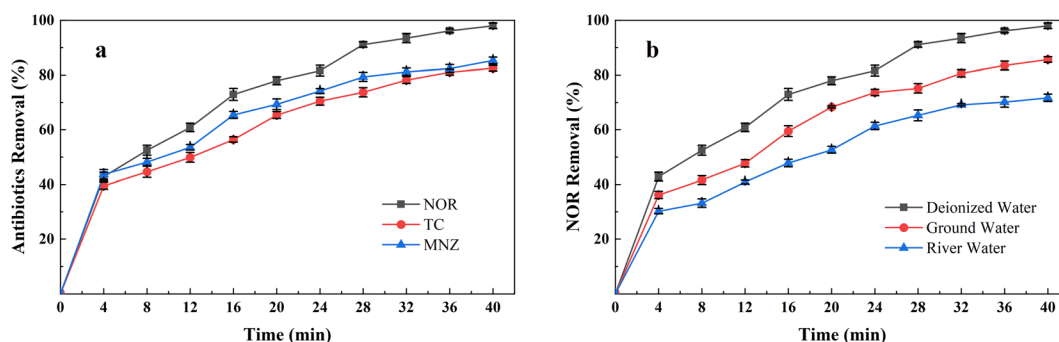


Fig. 10 (a) Removal of different antibiotics by AL-EC reactor and (b) influence of different water type on NOR removal; electrode combination, Fe anode and Al cathode, current density =  $2 \text{ mA cm}^{-2}$ , initial pH = 7, air flow rate =  $200 \text{ mL min}^{-1}$ , initial NOR = TC = MNZ =  $10 \text{ mg L}^{-1}$ .



Table 1 Compared the operating costs for treating antibiotics wastewater with present and other studies

Anode types	Pollutant types	Current density (mA cm <sup>-2</sup> )	Electricity consumption (kW h m <sup>-3</sup> )	Operation cost <sup>a</sup> (USD m <sup>-3</sup> )	References
Fe	Metronidazole	6	0.516	\	65
Al	Diclofenac	1.8	6.91	1.57	66
Stainless steel	Levofloxacin; ciprofloxacin	20	3.211	0.613	67
Fe	Tetracycline	4	0.110	0.177	68
Fe	Norfloxacin	2	0.388	0.153	This study

<sup>a</sup> Operation cost includes electrical energy consumption and the cost of dissolved Fe anode.

material consumption of electrode, which was calculated by the following equation:

$$\text{Operation cost}(\$) = a(E_{\text{EC}} + E_{\text{aeration}}) + bC_{\text{electrodes}} \\ = a \times t \times \frac{I \times U \times P \times V_{\text{aeration}}}{V_{\text{cell}}} + b \times \frac{I \times t \times M}{Z \times F} \quad (8)$$

where  $a$  is the average industrial electricity price in 2022 Chinese market (0.104 USD kW h<sup>-1</sup>),  $t$  is the treatment time (s),  $V_{\text{cell}}$  is the treated solution volume (m<sup>3</sup>),  $I$  is the applied current (A) and  $U$  is applied voltage (V),  $P$  is the power consumption of aeration (about 0.67 kW h m<sup>-3</sup>),  $V_{\text{aeration}}$  is the volume of aeration (m<sup>3</sup>).  $b$  is the local price of metal calculated by iron plate (0.634 USD kg<sup>-1</sup>),  $M$  is the molar mass of the metal (g mol<sup>-1</sup>),  $Z$  is the number of electrons involved in the redox reaction ( $Z = 2$  for iron),  $F$  is Faraday's constant (96 485 C mol<sup>-1</sup>). In general, the cost evaluation was carried out according to the optimal conditions: current density 2 mA cm<sup>-2</sup>, initial pH 7, treatment time 32 minutes and air flow rate of 200 mL min<sup>-1</sup> (Table 1).

## 6 Conclusions

In summary, the AL-EC reactor showed great potential for NOR removal from water, with low cost and high efficiency. The following optimal operating parameters were identified: iron anode and aluminum cathode combination, the current density of 2 mA cm<sup>-2</sup>, initial pH of 7, treatment time of 32 minutes and an air flow rate of 200 mL min<sup>-1</sup>, supporting electrolyte type was NaCl, initial NOR concentration of 10 mg L<sup>-1</sup>. The flocs were characterized using SEM, XRF, FT-IR, and XRD. Intermediate of NOR degradation was identified by LC-MS and proposed a possible degradation pathway during the electrocoagulation process. The results revealed that NOR removal mechanism was mainly due to electrochemical oxidation and floc adsorption. Using the optimal operating condition of the AL-EC reactor to treat the real water and different types of antibiotics, it was found that the minimum removal rate was over 60%, indicating its universality and adaptability. The operation cost under the optimum conditions was estimated at 0.153 USD m<sup>-3</sup>. This study shows that electrocoagulation combining airlift technology was an effective and cost-saving method for removing NOR or other antibiotic complexes from water. We hope that, by further optimizing the reactor design and operating parameters, the AL-EC technology can be applied for large-scale treatment of antibiotics or other organic wastewater.

## Author contributions

X. G Gu: conceptualization, methodology, software, data curation, writing – original draft preparation; X. T Feng, J. K. Wang and W. Y Qu: visualization, investigation; J. F Li: supervision, involved in conceptualization, methodology, software and english revising; W. Y Qu and W. H Wang: involved in software and validation.

## Conflicts of interest

The authors declare that they have no conflict of interest.

## Acknowledgements

Financial support from the National Natural Science Foundation of China (52260002, 42107414), the Special Application Science and Technology Project of the 7th Division in Xinjiang Bingtuan (2021A03008) and the Special Young Talented Research Project of Shihezi University (CXPY202201) are gratefully acknowledged.

## References

- 1 A. Bielen, A. Šimatović, J. Kosić-Vukšić, I. Senta, M. Ahel, S. Babić, T. Jurina, J. J. González Plaza, M. Milaković and N. Udiković-Kolić, *Water Res.*, 2017, **126**, 79–87.
- 2 E. Szekeres, A. Baricz, C. M. Chiriac, A. Farkas, O. Opris, M.-L. Soran, A.-S. Andrei, K. Rudi, J. L. Balcázar, N. Dragos and C. Coman, *Environ. Pollut.*, 2017, **225**, 304–315.
- 3 X.-L. Zhao, P. Li, C. Qu, R. Lu and Z.-H. Li, *Comp. Biochem. Physiol., Part C: Toxicol. Pharmacol.*, 2022, **258**, 109365.
- 4 P. T. P. Hoa, S. Managaki, N. Nakada, H. Takada, A. Shimizu, D. H. Anh, P. H. Viet and S. Suzuki, *Sci. Total Environ.*, 2011, **409**, 2894–2901.
- 5 J. Zhou and Q. Sun, *Polymers*, 2022, **14**, 3984.
- 6 J. He, Y. Zhang, F. Ni, D. Tian, Y. Zhang, L. Long, Y. He, C. Chen and J. Zou, *Sci. Total Environ.*, 2022, **831**, 154826.
- 7 Z. Wang, B. Song, J. Li and X. Teng, *Chemosphere*, 2021, **270**, 128652.
- 8 L. Miao, J. Li, L. Yi, W. Qu, C. Ma, X. Feng, Y. Xu and R. He, *J. Clean. Prod.*, 2022, **378**, 134421.
- 9 Y. Ma, Z. Wang, W. Yang, C. Chen, J. Li, R. He and S. Liu, *J. Water Process Eng.*, 2022, **49**, 103184.



- 10 X. Ma, Y. Cheng, Y. Ge, H. Wu, Q. Li, N. Gao and J. Deng, *Ultrason. Sonochem.*, 2018, **40**, 763–772.
- 11 A. Shahedi, A. K. Darban, F. Taghipour and A. Jamshidi-Zanjani, *Curr. Opin. Electrochem.*, 2020, **22**, 154–169.
- 12 S. Y. Lee and G. A. Gagnon, *Sep. Purif. Technol.*, 2016, **163**, 162–168.
- 13 N. Farhadian, J. Behin and A. Parvareh, *Comput. Fluids*, 2018, **167**, 221–228.
- 14 S. H. Ammar and A. S. Akbar, *Chin. J. Chem. Eng.*, 2018, **26**, 879–885.
- 15 J. Behin, N. Farhadian, M. Ahmadi and M. Parvizi, *J. Water Process Eng.*, 2015, **8**, 171–178.
- 16 N. Chawaloesphonsiya, C. Prommajun, K. Wongwailikhit and P. Painmanakul, *Environ. Technol.*, 2017, **38**, 1295–1304.
- 17 M. Bennajah, B. Gourich, A. H. Essadki, C. Vial and H. Delmas, *Chem. Eng. J.*, 2009, **148**, 122–131.
- 18 H. K. Hansen, P. Nuñez and C. Jil, *Sep. Sci. Technol.*, 2008, **43**, 212–224.
- 19 R. Elkacmi, O. Boudouch, A. Hasib, M. Bouzaid and M. Bennajah, *Sustain. Chem. Pharm.*, 2020, **17**, 100274.
- 20 N. Nippatla and L. Philip, *J. Environ. Manage.*, 2020, **273**, 111039.
- 21 A. Y. Goren, M. Kobya and M. S. Oncel, *Chemosphere*, 2020, **251**, 126363.
- 22 D. Balarak, M. Dashtizadeh, R. S. Oguike and K. Chandrika, *J. Pharm. Res. Int.*, 2020, **32**, 53–60.
- 23 M. Chafi, B. Gourich, A. H. Essadki, C. Vial and A. Fabregat, *Desalination*, 2011, **281**, 285–292.
- 24 M. Mechelhoff, G. H. Kelsall and N. J. D. Graham, *Chem. Eng. Sci.*, 2013, **95**, 301–312.
- 25 N. N. Abdulrazzaq, B. H. Al-Sabbagh and H. A. Shanshool, *J. Water Process Eng.*, 2021, **40**, 101906.
- 26 N. Galvão, J. B. de Souza and C. M. d. S. Vidal, *J. Environ. Chem. Eng.*, 2020, **8**, 104368.
- 27 M. H. Abdel-Aziz, E. S. Z. El-Ashtoukhy, M. S. Zoromba, M. Bassyouni and G. H. Sedahmed, *J. Ind. Eng. Chem.*, 2020, **82**, 105–112.
- 28 B. Xu, S. M. Iskander and Z. He, *Environ. Res.*, 2020, **182**, 109006.
- 29 L. Bilińska, K. Blus, M. Foszpańczyk, M. Gmurek and S. Ledakowicz, *J. Environ. Manage.*, 2020, **265**, 110502.
- 30 S. Fu, H. Jia, X. Meng, Z. Guo and J. Wang, *Sci. Total Environ.*, 2021, **781**, 146797.
- 31 M. H. Ibrahim, D. T. Moussa, M. H. El-Naas and M. S. Nasser, *J. Water Process Eng.*, 2020, **33**, 101091.
- 32 R.-F. Chen, L. Wu, H.-T. Zhong, C.-X. Liu, W. Qiao and C.-H. Wei, *Sep. Purif. Technol.*, 2021, **272**, 118900.
- 33 N. Huda, A. A. A. Raman, M. M. Bello and S. Ramesh, *J. Environ. Manage.*, 2017, **204**, 75–81.
- 34 C. M. van Genuchten, T. Behrends, P. Kraal, S. L. S. Stipp and K. Dideriksen, *Electrochim. Acta*, 2018, **286**, 324–338.
- 35 F. Akbal and S. Camcı, *Desalination*, 2011, **269**, 214–222.
- 36 M. Kobya, U. Gebologlu, F. Ulu, S. Oncel and E. Demirbas, *Electrochim. Acta*, 2011, **56**, 5060–5070.
- 37 B. Yang, Y. Han, Y. Deng, Y. Li, Q. Zhuo and J. Wu, *Emerg. Contam.*, 2016, **2**, 49–55.
- 38 M. Nasrullah, L. Singh, S. Krishnan, M. Sakinah, D. M. Mahapatra and A. W. Zularisam, *J. Water Process Eng.*, 2020, **33**, 101114.
- 39 H. Huang, D. Zhang, Z. Zhao, P. Zhang and F. Gao, *J. Clean. Prod.*, 2017, **141**, 429–438.
- 40 P. Song, Z. Yang, H. Xu, J. Huang, X. Yang and L. Wang, *Ind. Eng. Chem. Res.*, 2014, **53**, 12911–12919.
- 41 N. Muhammad Niza, M. S. Yusoff, M. A. A. Mohd Zainuri, M. I. Emmanuel, A. Mohamed Hussen Shadi and M. A. Kamaruddin, *J. Water Process Eng.*, 2020, **36**, 101282.
- 42 M. Ingelsson, N. Yasri and E. P. L. Roberts, *Water Res.*, 2020, **187**, 116433.
- 43 L. Q. Xu, X. J. Xu, G. Z. Cao, S. L. Liu, Z. Y. Duan, S. M. Song, M. Y. Song and M. J. Zhang, *J. Environ. Manage.*, 2018, **218**, 129–138.
- 44 Z. Guo, Y. Zhang, H. Jia, J. Guo, X. Meng and J. Wang, *Sci. Total Environ.*, 2022, **806**, 150529.
- 45 W. T. Mook, M. K. Aroua, M. Szlachta and C. S. Lee, *Water Sci. Technol.*, 2016, **75**, 952–962.
- 46 C. J. Izquierdo, P. Canizares, M. A. Rodrigo, J. P. Leclerc, G. Valentin and F. Lapique, *Desalination*, 2010, **255**, 15–20.
- 47 E. A. Serna-Galvis, K. E. Berrio-Perlaza and R. A. Torres-Palma, *Environ. Sci. Pollut. Res.*, 2017, **24**, 23771–23782.
- 48 M.-K. Kim, T. Kim, T.-K. Kim, S.-W. Joo and K.-D. Zoh, *Sep. Purif. Technol.*, 2020, **247**, 116911.
- 49 J. R. Silva, F. Carvalho, C. Vicente, A. D. Santos, R. M. Quinta-Ferreira and L. M. Castro, *J. Environ. Chem. Eng.*, 2022, **10**, 107750.
- 50 A. Oulebsir, T. Chaabane, H. Tounsi, K. Omine, V. Sivasankar, A. Flilissa and A. Darchen, *J. Environ. Chem. Eng.*, 2020, **8**, 104597.
- 51 M. Reilly, A. P. Cooley, B. Richardson, D. Tito and M. K. Theodorou, *J. Water Process Eng.*, 2021, **42**, 102121.
- 52 M. A. Sandoval, R. Fuentes, A. Thiam and R. Salazar, *Sci. Total Environ.*, 2021, **753**, 142108.
- 53 X. Lü, T. Xu, Y. Zhou, Q. Peng, J. Ou, B. Hu, Z. Xie, X. Lei and G. Yu, *J. Environ. Sci.*, 2023, **124**, 823–834.
- 54 Y. Zhong, C. Chen, S. Liu, C. Lu, D. Liu, Y. Pan, H. Sakiyama, M. Muddassir and J. Liu, *Dalton Trans.*, 2021, **50**, 18016–18026.
- 55 Y. Wang, W. Yu, Z. Chang, C. Gao, Y. Yang, B. Zhang, Y. Wang and B. Xing, *Sci. Total Environ.*, 2022, **848**, 157495.
- 56 L. Zhao, J. Liu, H. Wang and Y.-h. Dong, *Environ. Sci. Pollut. Res.*, 2019, **26**, 10685–10694.
- 57 P. Oulego, M. A. Villa-García, A. Laca and M. Diaz, *Dalton Trans.*, 2016, **45**, 9446–9459.
- 58 K. K. Aligizaki, M. R. de Rooij and D. D. Macdonald, *Cem. Concr. Res.*, 2000, **30**, 1941–1945.
- 59 K. Govindan, A. Angelin, M. Kalpana, M. Rangarajan, P. Shankar and A. Jang, *ACS Appl. Mater. Interfaces*, 2020, **12**, 1775–1788.
- 60 L. Yi, B. Li, Y. Sun, S. Li, Q. Qi, J. Qin, H. Sun, X. Wang, J. Wang and D. Fang, *Sep. Purif. Technol.*, 2021, **259**, 118166.
- 61 X. Chen, R. Zhuan and J. Wang, *J. Hazard. Mater.*, 2021, **404**, 124172.
- 62 F. Zhu, Y. Wu, Y. Liang, H. Li and W. Liang, *Chem. Eng. J.*, 2020, **389**, 124276.



- 63 H. Zhang, J. M. Bian, C. G. Yang, Z. C. Hu, F. Y. Liu and C. P. Zhang, *Sci. Total Environ.*, 2022, **810**, 151955.
- 64 Y. H. Zhou, B. N. Hu, X. J. Zhuang, J. X. Qiu, T. Xu, M. P. Zeng, X. He and G. Yu, *Sustainability*, 2022, **14**, 2328.
- 65 R. Zhou, F. Y. Liu, X. Y. Du, C. P. Zhang, C. G. Yang, N. A. Offiong, Y. H. Bi, W. Zeng and H. J. Ren, *Sep. Purif. Technol.*, 2022, **290**, 120799.
- 66 B. M. B. Ensano, L. Borea, V. Naddeo, V. Belgiorno, M. D. G. de Luna, M. Balakrishnan and F. C. Ballesteros, *J. Hazard. Mater.*, 2019, **361**, 367–373.
- 67 S. J. Mohammed, M. J. M-Ridha, K. M. Abed and A. A. M. Elgharbawy, *Int. J. Environ. Anal. Chem.*, 2021, 1–19, DOI: [10.1080/03067319.2021.1913733](https://doi.org/10.1080/03067319.2021.1913733).
- 68 S. Ahmadzadeh and M. Dolatabadi, *Chemosphere*, 2018, **212**, 533–539.

